Frontiers in Bioscience Landmark

Front. Biosci. (Landmark Ed) **2025**; 30(6): 37494
https://doi.org/10.31083/FBL37494

Original Research

Cobalt Chloride-simulated Hypoxia Promoted Ossification of the Posterior Longitudinal Ligament Through the HIF1A–BMP4 Axis

Shihao Lu[1,†], Junbin Liu[1,†], Junzhe Sheng[1], Aochen Xu[1], Zichuan Wu[1], Chen Xu[1], Jiabin Yuan[2,*], Yang Liu[1,*]

[1]Department of Orthopedics, Changzheng Hospital, Naval Medical University, 200003 Shanghai, China
[2]Department of Spine Surgery, Changhai Hospital, Naval Medical University, 200433 Shanghai, China
*Correspondence: smmuyuan@163.com (Jiabin Yuan); liuyangspine@hotmail.com (Yang Liu)
[†]These authors contributed equally.
Academic Editor: Elisa Belluzzi
Submitted: 5 February 2025 Revised: 26 April 2025 Accepted: 7 May 2025 Published: 23 June 2025

Abstract

Background: The ossification of the posterior longitudinal ligament (OPLL) is a progressive spinal disorder predominantly observed in Asian populations. Unfortunately, there is a limited availability of conservative therapies to impede the progression of OPLL. This study investigates the effects of cobalt chloride ($CoCl_2$), which simulates an *in vitro* hypoxic microenvironment, on OPLL and explores its potential mechanisms, aiming to enhance our understanding of the pathogenesis of OPLL. **Methods**: Ligament cells were extracted from patients with OPLL and normal posterior longitudinal ligament (PLL) tissues, confirming their mesenchymal stem cell (MSC)-like properties. To simulate hypoxia, cells were treated with varying concentrations of $CoCl_2$, and the effects on hypoxia-inducible factor 1-alpha (HIF1A) expression and osteogenic differentiation were assessed. Real-time quantitative reverse transcription–polymerase chain reaction (qRT-PCR) and Western blotting were used to quantify HIF1A and bone morphogenetic protein 4 (BMP4) expression. Immunohistochemistry was performed to visualize HIF1A in tissue samples. Osteogenic differentiation was evaluated through Alizarin Red S staining and alkaline phosphatase (ALP) assays, with optical density (OD) values measured using a microplate reader. Transcriptome sequencing was conducted to identify differentially expressed genes following $CoCl_2$ treatment. **Results**: We found that HIF1A was differentially expressed in the OPLL. Both PLL cells and OPLL cells exhibited mesenchymal stem cell properties; however, OPLL cells demonstrated a greater capacity for osteogenic differentiation ($p < 0.05$). Following stimulation with cobalt chloride, the expression of HIF1A increased, which correlated with an enhanced osteogenic differentiation ability in PLL cells. Biosignature analysis revealed that HIF1A plays a regulatory role in BMP4 expression. Notably, BMP4 was downregulated, and the degree of osteogenic differentiation decreased upon inhibition of HIF1A with siRNA in OPLL cells. **Conclusions**: Primary cells derived from normal PLL and OPLL exhibited MSC-like properties and demonstrated the capacity for osteogenic, adipogenic, and chondrogenic differentiation, with OPLL cells showing a greater propensity for osteogenic differentiation. This study reports the potential involvement of HIF1A in the development of OPLL and investigates the regulatory role of the HIF1A-BMP4 axis in this process.

Keywords: ossification of the posterior longitudinal ligament; hypoxia; HIF1A; *in vitro*

1. Introduction

Ossification of the posterior longitudinal ligament (OPLL) is a common spinal condition characterized by heterotopic spinal ossification [1]. In the early stages of OPLL, this ossification exerts pressure on the spinal cord, leading to symptoms such as numbness in the limbs [2,3] and abnormalities in urination and defecation [4]. In severe cases, even minor accidents can lead to paralysis. Current treatments are often inadequate because early detection does not halt the progression of ossification. Therefore, research into the pathogenesis of OPLL is essential to prevent the formation and progression of ossification. Furthermore, re-ossification and associated complications may persist even after surgical intervention [5]. The incidence of OPLL is currently increasing annually, making surgical treatment a complex, costly and challenging endeavor with numerous drawbacks [6].

Although the fundamental aspect of OPLL is heterotopic ossification (HO), defined as the presence of bone tissue within muscle or connective tissue, the exact pathogenesis remains unclear. OPLL specifically refers to the segment of the spine where bone tissue replaces the posterior longitudinal ligament (PLL). Three key factors are required for HO to occur: osteogenic progenitor cells, inducing factors and their associated signaling pathways, and a suitable microenvironment. In particular, an appropriate hypoxic microenvironment is essential for the initiation of HO [7].

The development of OPLL is a complex process characterised by neovascularisation and proliferation of *in situ* cells within the ligament. These changes lead to degeneration and hypertrophy of the PLL, ultimately leading to the formation of mature platelet-like bone [8]. Hypoxia plays a critical role as a cellular physiological response and is essential for the initiation of ossification [9].

Hypoxia-inducible factor 1α (HIF1A) is a transcription factor that regulates the cellular response to hypoxia and consists of an oxygen-regulated alpha subunit and a constitutively expressed beta subunit. HIF1A is critical in determining HIF-1 transcriptional activity and directly targets hundreds of genes, including those encoding vascular endothelial growth factor (VEGF), bone morphogenetic proteins (BMPs) and runt-related transcription factor 2 (RUNX2) [10–12], which are involved in osteogenic and angiogenic differentiation. Cobalt chloride ($CoCl_2$) is a widely used chemical hypoxia mimetic that competes with divalent ions to inhibit the formation of oxygenated hemoglobin [13]. $CoCl_2$ inhibits prolyl hydroxylase catalysis and induces an intracellular hypoxia-like state in cell cultures [14]. This method more accurately simulates a hypoxic microenvironment and provides greater stability compared to other hypoxia simulation techniques.

Bone morphogenetic protein 4 (BMP4) is recognized as one of the genetic determinants associated with patients suffering from OPLL. BMP4 serves as a biomarker for this condition, particularly in the context of spinal ossification. In Asian populations affected by OPLL, novel mutations and specific haplotypes of the *BMP4* gene have been identified as contributing factors that increase the risk of developing this disorder. In particular, the presence of the T allele at position 6007 in the *BMP4* gene may serve as a significant risk factor for cervical OPLL, particularly in Han male patients.

Despite these associations, the precise pathogenesis of BMP4 in the context of the posterior longitudinal ligament remains unexplored. Previous studies have shown that BMP4 promotes OPLL under mechanical stress stimulation [15,16] and is the only gene to meet the criteria for suggestive evidence of association from a large-scale OPLL candidate gene screen [17,18]. In our study, high-throughput sequencing results indicated that HIF1A can regulate several differentially expressed genes related to ossification following hypoxic conditions in PLL cells. Both protein-protein interaction (PPI) network analysis and transcription factor targeting analysis suggested that HIF1A has the potential to regulate BMP4. Therefore, we selected BMP4 for further investigation in our research.

We hypothesize that hypoxia influences the development of OPLL and that HIF1A may play an important role in this process. However, there have been no reports investigating the relationship between OPLL and hypoxia. Our aim was to establish an *in vitro* hypoxia model using $CoCl_2$ to investigate the changes in HIF1A expression under hypoxic conditions by culturing primary cells and thereby elucidate the potential mechanisms underlying hypoxia-mediated OPLL.

2. Materials and Methods

2.1 Primary Cell Culture and Sample Collection

The identification of OPLL or PLL in patients with spinal trauma who received cervical corpectomy was validated preoperatively through CT (iCT 256; Philips Medical Systems, Best, Netherlands) and MRI (Magnetom Skyra, Siemens Healthcare, Germany) at our facility. Specimens of OPLL or PLL obtained during the surgical procedure were promptly placed into primary cell culture, as outlined in previous research [9]. In summary, the ligaments were washed twice with PBS (Servicebio, Wuhan, China) and then meticulously dissected under microscopic observation to prevent contamination with bone or disc material. The excised tissues were minced, rinsed, and cultured in a 100-mm dish filled with Dulbecco's modified Eagle's medium (DMEM, Life Technology Gibco, Grand Island, NY, USA), enriched with 10% fetal bovine serum (FBS; Gibco, Rockville, MD, USA), 1% L-glutamine (Gibco, USA), and 1% penicillin/streptomycin (Gibco, USA), in a humidified environment consisting of 95% air and 5% CO_2 at a temperature of 37 °C. The migrating fibroblast-like cells were collected using 0.02% EDTA/0.05% trypsin (Gibco, USA) and then transferred to a T25 culture flask for further growth and analysis. The research protocols received approval from the Shanghai Changzheng Hospital Biomedical Research Ethics Committee, and all participants or their families/legal guardians gave written informed consent. The procedures adhered to the established ethical guidelines. We acquired three tissue samples from patients with OPLL during an anterior cervical discectomy and three control samples from individuals with PLL during an anterior cervical corpectomy. All cell lines were validated by STR profiling and tested negative for mycoplasma.

2.2 Construction of Cell Hypoxia Model

The selected cell lines were cultured in an appropriate medium at 37 °C in a 5% CO_2 incubator until they reached 70%–80% confluence [19]. Under sterile conditions, cobalt chloride (Sigma-Aldrich, St.Louis, MO, USA) was dissolved in PBS buffer to prepare solutions of varying concentrations (0, 50, 100, and 200 μM) for subsequent experimental use [20]. The cultured cells were washed once with PBS buffer to eliminate any residual components from the medium. The pre-prepared cobalt chloride solutions were then added to each well, establishing different treatment groups, including control groups and those treated with varying concentrations of cobalt chloride, with a minimum of three replicates for each group. The treated cells were incubated at 37 °C in a 5% CO_2 environment for either 24 or 48 hours, depending on the specific requirements of the experimental design. To assess the hypoxic response, HIF1A was utilized as a key indicator.

Table 1. Nucleotide sequences of the primers.

Primer name	Sequence (5′ to 3′)
HIF1-F	AAGTCAGCAACGTGGAAGGT
HIF1-R	ATCAGCACCAAGCACGTCAT
BMP4-F	TCCTCTTTAACCTCAGCAGCATCC
BMP4-R	GTCTCGTGTCCAGTAGTCGTGTG
RUNX2-F	AAGCCAAACACAAACAGCGGAAAC
RUNX2-R	CGTCAAGGTACAGCATCGAGATAGC
OCN-R	GTCCCGGATGTAACTGGTGTC
OCN-F	CTACTTGGACCATAATGCCCTG
β-actin-F	CCACGAAACTACTTCAACTCCATC
β-actin-R	AGTGATCTCCTTCTGCATCCTGTC

HIF1, hypoxia-inducible factor 1; BMP4, bone morphogenetic protein 4; RUNX2, runt-related transcription factor; OCN, osteocalcin.

2.3 Real-time Quantitative Reverse Transcription–Polymerase Chain Reaction (qRT-PCR)

Total RNA was extracted from PLL and OPLL cells using TRIzol (Invitrogen, Carlsbad, CA, USA) and then converted into cDNA with the help of a PrimeScript RT reagent kit (TaKaRa, Kyoto, Japan). qRT-PCR was performed on a LightCycler 480 PCR system (Roche, BSL, Switzerland) employing SYBR Premix Ex Taq (TaKaRa, Kyoto, Japan). Expression values were normalized to those of β-actin. The experiment was independently repeated three times. The relative expression levels of the genes were determined using the comparative threshold cycle ($2^{-\Delta\Delta CT}$) method. The forward and reverse primers were purchased from Shanghai Sangong Biotechnology (Shanghai, China) and each gene are presented in Table 1.

2.4 Western Blotting

Proteins were isolated following the manufacturer's guidelines utilizing a commercial kit (No. C510003, Sangon Biotech, Shanghai, China). The primary antibodies employed included rabbit anti-HIF1A (ab51608, Abcam, Beverly, MA, USA), rabbit anti-BMP4 (ab124715, Abcam, USA), and rabbit anti-β-actin (ab8227, Abcam, USA), each diluted to 1:1000. A 10% sodium dodecyl sulfate polyacrylamide gel electrophoresis (SDS-PAGE) (Beyotime, Shanghai, China) was used to separate the protein samples, which were then transferred to nitrocellulose filter membranes (Pall Corp., Washington, NY, USA) via a wet transfer blotting system (Bio-Rad, Hercules, CA, USA). After incubation, the secondary antibody, goat anti-rabbit HRP (RGAR001, Proteintech, China), was introduced at a dilution of 1:2000. Protein detection was carried out with a chemiluminescence detection system (Millipore, Billerica, MA, USA). The mean intensity (intensity/area) of bands was determined and normalized against anti-β-actin using ImageJ software (V1.8.0.112, National Institutes of Health, Bethesda, MD, USA), and the experiment was independently repeated three times.

2.5 Immunohistochemistry Analysis

Tissues from PLL/OPLL were preserved in 4% paraformaldehyde (PFA, Beyotime, China) for a duration of 24 hours and then rinsed three times with PBS. The samples were subjected to decalcification, dehydration, and embedding in OCT compound, followed by obtaining 10 µm cryosections via a cryostat. The sections were treated to permeabilization and blocking in TBST (Biosharp, Hefei, China) supplemented with 0.3% Triton X-100 (Sigma-Aldrich, St.Louis, MO, USA) and 5% bovine serum albumin (Gibco, USA). Subsequently, the sections were treated with anti-HIF1A antibody (ab51608, Abcam, USA) overnight at 4 °C and were later incubated with goat anti-rabbit secondary antibody (1:300, ab6721, Abcam, USA) for 1 hour at room temperature. For nuclear visualization, 4,6-diamidino-2-phenylindole (DAPI, Abcam, USA) was used as a counterstain for 5 minutes.

In the process of performing immunofluorescence staining on cultured cells, fixed cells underwent several steps, including permeabilization, blocking, and overnight incubation with the primary antibodies. This was subsequently followed by a one-hour incubation with the relevant secondary antibodies. The primary antibodies used for the immunofluorescence staining comprised rabbit anti-RUNX2 (1:100; ab76956, Abcam, USA), rabbit anti-vimentin (1:100; 80232-1-RR, Proteintech, Wuhan, China), rabbit anti-HIF1A (1:100; ab51608, Abcam, USA), rabbit anti-BMP4 (1:100; ab124715, Abcam, USA), and rabbit anti-OCN (1:100; ab133612, Abcam, USA). For the secondary antibodies, goat anti-rabbit IgG H&L (Alexa Fluor 488) (1:200; ab150077, Abcam, USA) and goat anti-rabbit IgG H&L (Alexa Fluor 594) (1:200; ab150080, Abcam, USA) were utilized. The experiment was independently repeated three times. Image taken with Leica Thunder high resolution fluorescence microscope (DMi8, Wetzlar, Germany).

2.6 Cell Proliferation Assay

Cell proliferation was evaluated employing the cell counting kit-8 (CK04-11, Dojindo Laboratories, Kumamoto, Japan). The growth medium consisted of DMEM (12-604F, Lonza, Basel, Switzerland), enriched with 10% FBS and antibiotics. After a 2-hour incubation period, cells were treated with 10 µL of cell counting kit-8 (CCK-8) reagent for staining. The absorbance levels were measured at 450 nm using an enzyme-labeler (Bio-Rad Laboratories, Hercules, CA, USA). The number of surviving cells was calculated using Image J software (V1.8.0.112, National Institutes of Health, Bethesda, MD, USA).

In the live-dead cell staining experiment, a cell suspension was prepared by collecting cells through digestion centrifugation. A working solution for staining (100 µL), created following the guidelines of the Calcein-AM/PI Live Cell/Dead Cell Double Staining Kit (Solarbio, Beijing, China), was mixed with 200 µL of the cell suspension and

then incubated at 37 °C for 15 minutes. The presence of live cells was assessed based on their green fluorescence (488 nm), whereas dead cells were identified through their red fluorescence (550 nm) when observed under Leica Thunder high resolution fluorescence microscope (DMi8, Wetzlar, Germany).

2.7 Alizarin Red S (ARS) and Alkaline Phosphatase Staining and Quantification

Prior to examining the osteogenic characteristics of the cells, they were subjected to osteogenic induction medium comprising DMEM supplemented with 10% FBS, 25 mg/mL ascorbate-2 phosphate, 100 nM dexamethasone, and 5 mM β-glycerophosphate (all sourced from Gibco, USA) for the specified duration (or, alternatively, 2 weeks). Following induction, the cells were fixed in a 4% PFA (Beyotime, China) solution with 15 minutes, rinsed with PBS three times (Servicebio, China), and stained according to the guidelines provided by the manufacturer. Calcium deposition was assessed utilizing an ARS Staining Kit (#0223, ScienCell, San Diego, CA, USA) and quantified with the help of an ARS Staining Quantification Assay kit (#8678, ScienCell, San Diego, CA, USA). The cellular alkaline phosphatase (ALP) was evaluated using an ALP staining kit (1102-100, Sidansai, Shanghai, China) and its quantification was carried out with an ALP assay kit (ab83369, Abcam, USA). The optical density (OD) at 405 nm for each sample was determined, with the background control represented by the mean OD at 570 nm of each sample. To obtain a standardized optical density value for comparative purposes, the OD at 405 nm was divided by that at 570 nm. Absorbance measurements were performed using an Infinite™ M200 microplate reader (Tecan, Ocala, FL, USA), and results were averaged from three replicates.

2.8 Adipogenic and Chondrogenic Differentiation

Differentiation into adipocytes was initiated with the administration of 1 µM dexamethasone, 10 µg/mL insulin (Humalog; Novo Nordisk, Bagsvaerd, Denmark), 200 µM indomethacin (17378; Sigma-Aldrich, St.Louis, MO, USA), and 500 µM IBMX (I5879; Sigma-Aldrich, St.Louis, MO, USA). The formulation for chondrogenic differentiation included 100 nM dexamethasone, 50 µM ascorbic acid, 10 ng/mL TGF-β3 (8791; Merck Millipore, Darmstadt, Germany), and 10 µM insulin. For both osteogenesis and adipogenesis, a density of 1.5×10^4 cells per well was seeded into 6-well culture plates and maintained for a maximum of 21 days at 37 °C. After induction, it was washed three times with PBS, fixed with 4% paraformaldehyde for 15 minutes, and then washed with PBS for three times before staining. Mineralization was assessed via ARS staining (A5533; Merck Millipore, Darmstadt, Germany), whereas lipid droplets were examined using oil red O staining (O0625; Merck Millipore, Darmstadt, Germany). To evaluate chondrogenesis, the cell pellets were subjected to Alcian blue staining (A9186; Merck Millipore, Darmstadt, Germany) following a culture duration of six weeks.

2.9 Flow Cytometric Analysis

Flow cytometry was performed with a FACSCanto II and analyzed using FACSDiva software (V9.0, BD Biosciences, San Jose, CA, USA). The posterior longitudinal ligament cells (PLLCs) were maintained in 100-mm petri dishes and collected once they reached 70% confluency. For analysis, the cells were resuspended in PBS at a density of 1×10^6 cells/mL. To assess stemness, the expression of various cell surface markers was evaluated in a 10 µL sample. The experiment was independently repeated three times. All reagents necessary for flow cytometry, including CD11b-PE (BD561355), CD105-PE (BD560839), CD44-PE (BD566803), and CD73 (BD560199), were sourced from BD Biosciences (USA).

2.10 RNA-seq Analysis

RNA extraction was performed after a three-day culture of PLLCs. Sequencing of the RNA (RNA-seq) was carried out on all cells obtained from both control and OPLL patients. The synthesis of cDNA, preparation of the library, and RNA-seq were completed on an Illumina HiSeq 2000 by Macrogen, located in Seoul, Korea [21]. For the following analysis, Fragments Per Kilobase of transcript per Million mapped reads (FPKM) values and raw read count data were collected. R software (version 4.1.2; https://www.r-project.org/) was utilized for statistical analyses, and the related package-driven analyses along with graphical diagrams were created using ggplot2 (https://ggplot2.tidyverse.org/). Using the limma R package (https://www.bioconductor.org/packages/release/bioc/html/limma.html), we identified differentially expressed genes (DEGs) between two risk groups according to the following conditions: $\log2|FC| > 1$, an adjusted p-value < 0.05 and a false discovery rate (FDR) < 0.05.

2.11 Transcription Factor Binding Site Prediction

The upstream 3000-bp region sequence files, starting from the transcription start site of the gene of interest, were retrieved from the UCSC Genome Browser (http://genome.ucsc.edu/). Relevant motif files for the transcription factors were sourced from the JASPAR database (https://jaspar.genereg.net/). The identification of transcription factor binding motifs within the promoter's upstream region of the target gene was performed using the FIMO online tool (https://meme-suite.org/meme/tools/fimo).

2.12 RNA Interference

High-throughput mRNA sequencing (RNA-seq) enables comprehensive measurement of the entire transcriptome through massive read production [21–23]. This technique allows for the analysis of DEGs, novel genes, alternative splice isoforms, and rare transcripts [24,

25]. siHIF1A was synthesized utilizing two specific sequences: 5′-CCGUAUGGAAGACAUUAAATT-3′ and 5′-UUUAAUGUCUUCCAUACGGTT-3′ (synthesized by Genepharma, Shanghai, China). The transfection procedure was performed with Lipofectamine RNAiMAX (Thermo Fisher Scientific, Waltham, Massachusetts, USA) following the recommended guidelines. In summary, the mesenchymal stem cells (MSCs) were plated and subsequently transfected with the siRNAs in conjunction with Lipofectamine RNAiMAX once they reached 70–90% confluence. Relevant experiments were executed on the tenth day of induction. The sequences of si-NC used are shown as follows:

S: 5′-UUCUCCGAACGUGUCACGUTT-3′

AS: 5′-ACGUGACACGUUCGGAGAATT-3′

2.13 Protein-protein Interaction Networks (PPI) Analysis

Using the Search Tool for the Retrieval of Interacting Genes Database (STRING) (https://cn.string-db.org/) [26], we identified all proteins that directly interact with HIF1A. These interactions are represented as non-directed edges connecting the protein nodes. The resulting PPI networks were constructed and visualized utilizing Cytoscape version 3.9.0 (https://github.com/cytoscape).

2.14 Statistical Analysis

Analysis of the data was conducted using SPSS (version 16.0, Chicago, IL, USA) software (https://www.ibm.com/products/spss-statistics) and GraphPad Prism (version 9.5.1, San Diego, CA, USA) software (https://www.graphpad.com). Where applicable, Student's *t*-test and one-way analysis of variance (ANOVA) with Tukey's post hoc test was utilized for assessing the differences of mean values of more than two groups. The results are expressed as mean values ± SEM. A *p*-value of less than 0.05 was deemed to be statistically significant.

3. Results

3.1 PLLCs/OPLLCs Exhibited MSC-like Properties

PLL tissues were extracted from three control subjects and three patients with OPLL, followed by the isolation, culture, and expansion of primary cells. Light microscopic observation revealed that the isolated PLLCs and OPLLCs were either pike-shaped or flat stellate cells, characterized by protrusions and nuclei with a regular ovoid shape (Fig. 1A). The validity of the primary culture was confirmed using immunofluorescence to assess the expression of the fibroblast-specific marker protein vimentin. The isolated PLLCs and OPLLCs exhibited positive staining for vimentin (Fig. 1B). These cells served as precursors to ossified material and possessed differentiation potential. The differentiation capability was evaluated through the mesenchymal immunophenotypic detection of MSCs using flow cytometry, revealing that both cell groups were positive for CD105, CD73, and CD44, while negative for CD11b (Fig. 1C,D).

The differentiation potential of the PLLCs and OPLLCs was assessed by inducing differentiation with osteogenic, adipogenic, and chondrogenic induction media. After three weeks, osteogenesis in PLLCs and OPLLCs was evaluated using ALP and ARS staining, while adipogenesis was assessed with oil red O staining. The cartilaginous properties were analyzed using Alcian blue staining, which indicated that both PLLCs and OPLLCs could differentiate into bone, adipose, and cartilage (Fig. 1E). Ossification was quantified through ARS absorbance measurement and ALP activity assays, revealing that OPLLCs exhibited a higher osteogenic differentiation capability compared to PLLCs (Fig. 1F,G). All extracted progenitor cells demonstrated characteristics consistent with MSC-like properties, with OPLLCs displaying comparatively stronger osteogenic properties.

3.2 HIF1A Exhibited Differential Expression Between PLL and OPLL

Hypoxia is believed to initiate HO, with HIF1A playing a crucial role in hypoxic microenvironments. We obtained tissues from patients undergoing surgery for PLL and OPLL and analyzed HIF1A expression using immunohistochemistry. The results revealed that HIF1A expression was significantly higher in OPLL tissues compared to normal PLL tissues (Fig. 2A,B). Furthermore, we performed a simultaneous examination of HIF1A expression in primary cells derived from both OPLL and PLL patients. The western blotting results indicated that HIF1A expression was comparatively higher in OPLLCs than in PLLCs (Fig. 2C,D). These findings suggest variations in HIF1A expression between PLL and OPLL patients both *in vitro* and *in vivo*.

3.3 $CoCl_2$-modelled Hypoxic Environment Promoted PLLC HIF1A Expression and Osteogenesis

$CoCl_2$ effectively mimics the hypoxic microenvironment *in vivo* and is widely utilized to investigate hypoxia. We stimulated PLLCs with 0, 50, 100, and 200 μM $CoCl_2$ and assessed HIF1A protein expression levels through western blotting. The results indicated that HIF1A protein expression increased following 24 and 48 hours of $CoCl_2$ stimulation (Fig. 3A,B). The impact of $CoCl_2$ on PLLCs proliferation was evaluated using the CCK-8 assay. While 50 and 100 μM $CoCl_2$ exhibited minimal effects, 200 μM $CoCl_2$ significantly impaired PLLCs proliferation (Fig. 3E). Furthermore, cell survival at 24- and 48-hours post-stimulation was assessed using calcein-AM/PI staining, which revealed an increase in dead cells under the 200 μM $CoCl_2$ conditions (Fig. 3C,D). We concluded that 48 hours of stimulation with 100 μM $CoCl_2$ effectively enhanced PLLCs HIF1A expression without adversely affecting cellular viability, suggesting that this concentration is optimal for stimulation.

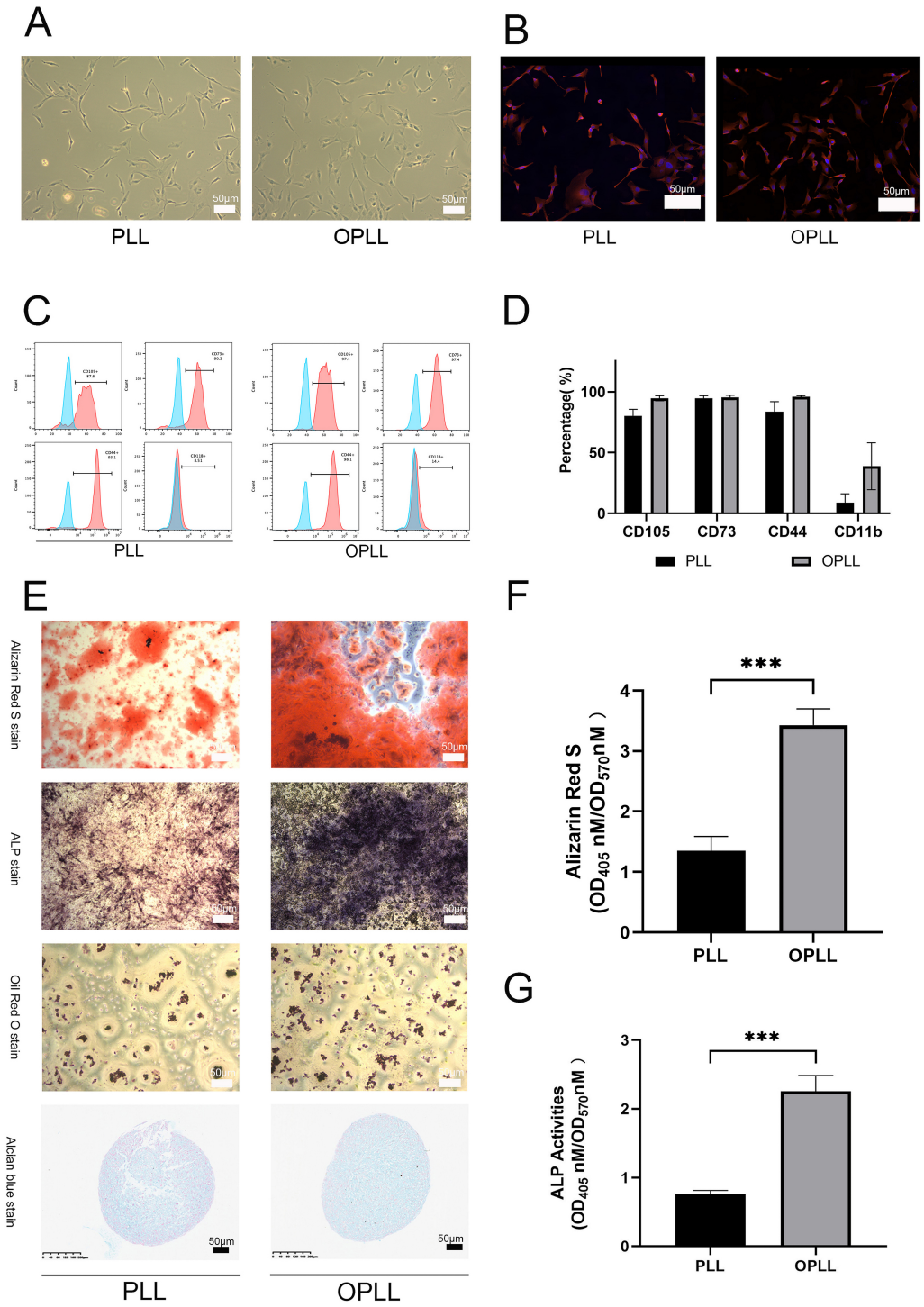

Fig. 1. Phenotypic features of PLLCs and OPLLCs. (A) Inverted microscopic live images of PLLCs and OPLLCs (×200) (n = 3/group). (B) Fluorescence microscopic live cell images of anti-vimentin antibody (red) staining and 4,6-diamidino-2-phenylindole (DAPI) nuclear counterstaining (blue) in PLLCs and OPLLCs (n = 3/group). (C) Analysis of CD105, CD73, CD44, and CD11b expression in PLLCs (n = 3/group) and OPLLCs (n = 3/group) in immunophenotypic study to define mesenchymal stem cells (MSCs). (D) Quantitative mapping of PLLCs and OPLLCs surface markers. (E) Staining results of PLLCs and OPLLCs after 3-week induction in osteogenic, adipogenic, and chondrogenic medium (n = 3/group). (F) Absorbance measurement of dissolved Alizarin Red S (ARS) at 405 and 507 nm in PLLCs and OPLLCs. (G) Absorbance measurement of dissolved alkaline phosphatase (ALP) at 405 and 507 nm in PLLCs and OPLLCs. All experiments were performed in triplicate, and the data are the mean ± SEM; *** $p < 0.001$ within groups. Scale bar: 50 μm. PLL, posterior longitudinal ligament; OPLL, ossification of the posterior longitudinal ligament; PLLCs, posterior longitudinal ligament cells; OPLLCs, ossification of the posterior longitudinal ligament cells.

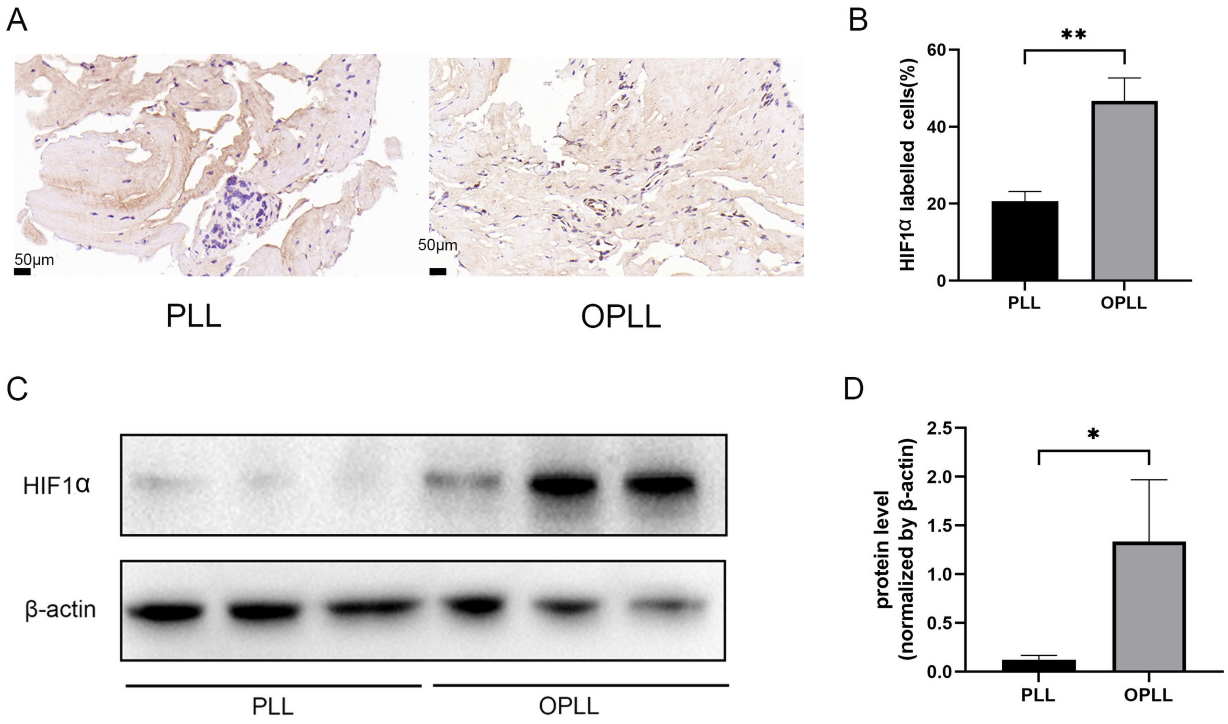

Fig. 2. Hypoxia-inducible factor 1-alpha (HIF1A) expression in PLL and OPLL. (A) Immunohistochemistry detection of HIF1A expression in PLL and OPLL tissue (n = 3/group). (B) Immunohistochemical staining demonstrating the ratio of positive cells to total tissue cells. (C) Western blot detection of HIF1A protein expression levels in primary cells from PLL and OPLL tissues (n = 3/group) and (D) ImageJ quantification of protein expression levels. All experiments were performed in triplicate, and the data are the mean ± SEM; * $p < 0.05$, ** $p < 0.01$ within groups. Scale bar: 50 μm.

The effect of HIF1A on ossification was investigated by inducing osteogenesis and HIF1A expression in PLLCs using a 100 μM $CoCl_2$ osteogenic medium. In contrast, HIF1A expression during osteogenesis induction in OPLLCs was inhibited using siRNA. Measurement of ossification through ARS and ALP staining indicated that osteogenic differentiation was significantly enhanced in PLLCs and OPLLCs within the $CoCl_2$-mimicked hypoxic microenvironment compared to untreated PLLCs ($p < 0.05$). Furthermore, the inhibition of HIF1A expression resulted in a reduction of osteogenesis in OPLLCs ($p < 0.05$) (Fig. 3F). Immunofluorescence staining demonstrated that $CoCl_2$ stimulation elevated the expression of osteogenic markers RUNX2 and osteocalcin (OCN) in PLLCs, while HIF1A inhibition led to a decrease in their expression in OPLLCs ($p < 0.05$) (Fig. 3G). To elucidate the precise mechanism by which the hypoxic microenvironment promotes OPLL, the transcriptome of PLLCs was sequenced using second-generation sequencing technology following $CoCl_2$ stimulation.

3.4 $CoCl_2$-modelled Hypoxic Stimulation Enhanced the HIF1A Pathway

In this study, we sequenced the transcriptomes of PLLCs derived from PLL tissues, both before and after $CoCl_2$ treatment. The Pearson correlation coefficients between the expression levels of any two samples were calculated, and the correlations between each pair were visualized using a heatmap (Fig. 4A). The sequencing results revealed differential gene expression following $CoCl_2$ stimulation, with adjustments indicating that 166 genes were upregulated, and 86 genes were significantly upregulated based on the thresholds of FDR <0.05, $p < 0.05$, and |log2 (fold change [FC])| ≥1 (Fig. 4B). Gene Ontology (GO) analysis indicated significant reshuffling of genes across biological processes, molecular functions, and cellular components (Fig. 4C). Notably, most of the top 10 GO terms were associated with altered oxygen levels (Fig. 4D). Additionally, Kyoto Encyclopedia of Genes and Genomes (KEGG) analysis revealed enriched pathways associated with differential genes, particularly highlighting the HIF-1 signaling pathway, which exhibited a significant enrichment of differential genes. The transcriptome sequencing of $CoCl_2$, which mimics a hypoxic microenvironment, demonstrated successful results, with differential gene expression primarily enriched in the hypoxia and HIF1A signaling pathways (Fig. 4E).

3.5 HIF1A Might Modulate BMP4 to Affect OPLL

The regulation of HIF1A in relation to OPLL was investigated by screening differential genes in the PLLCs and

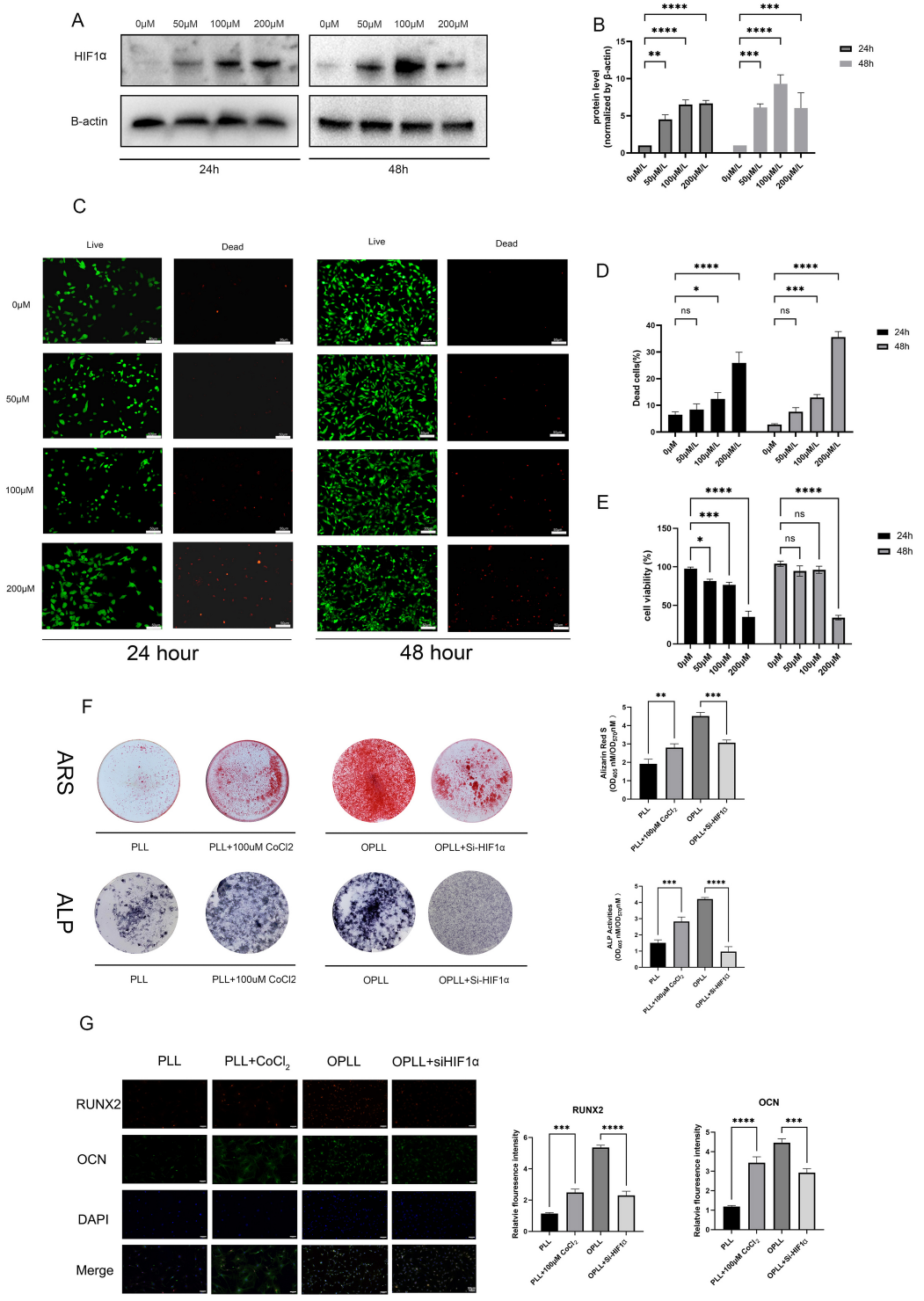

Fig. 3. A cobalt chloride ($CoCl_2$)-modelled hypoxic environment promotes PLLCs HIF1A expression and osteogenesis. (A) HIF1A protein expression levels in $CoCl_2$-stimulated PLLCs (n = 3/group) and (B) ImageJ quantification. (C) Calcein-AM/PI detection of PLLCs survival in normal medium and medium containing $CoCl_2$ (n = 3/group) and (D) the percentage of dead cells. (E) Cell counting kit-8 (CCK-8) assay of viability of $CoCl_2$-stimulated PLLCs (n = 3/group). (F) Osteogenic differentiation of PLLCs was induced with normal medium and medium containing 100 μM $CoCl_2$ and the degree of ossification was detected by ARS and ALP staining and quantified by the absorbance of dissolved ARS and ALP (n = 3/group). (G) Immunofluorescence detection of RUNX2 and OCN (n = 3/group). All experiments were performed in triplicate, and data are the mean ± SEM; ns was not statistically significant, * $p < 0.05$, ** $p < 0.01$, *** $p < 0.001$, **** $p < 0.0001$ within groups. Scale bar: 50 μm. RUNX2, runt-related transcription factor 2; OCN, osteocalcin; DAPI, 4',6-Diamidino-2-phenylindole.

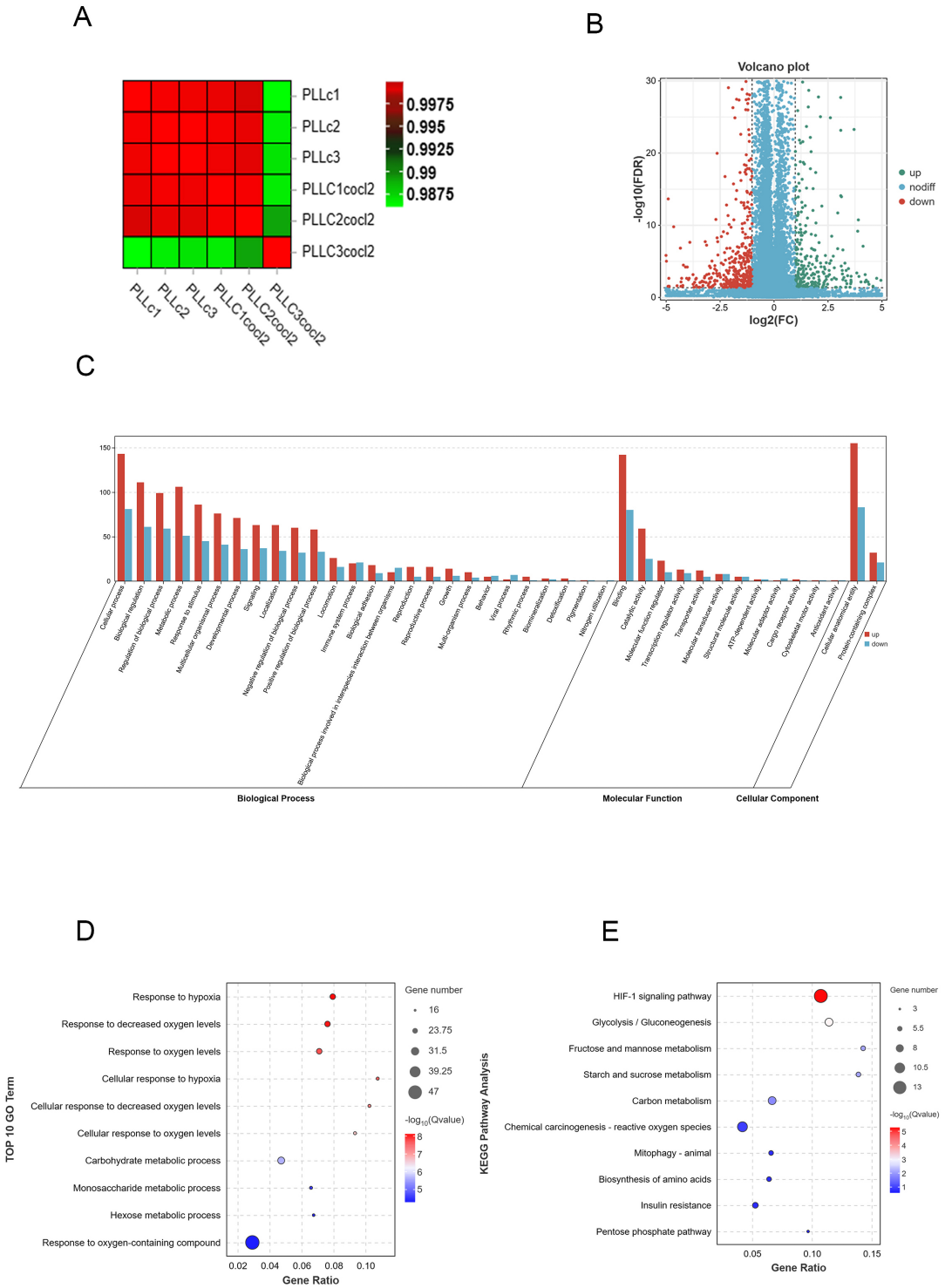

Fig. 4. RNA-seq analysis results of PLLCs (*n* = 3/group) and $CoCl_2$-stimulated PLLCs (PLLC $CoCl_2$) (*n* = 3/group). (A) Principal component analysis was performed to cluster patients based on major components. (B) Volcano plots depicting the mRNA expression profiles of PLLCs cultured in standard medium and $CoCl_2$ medium. (C) Gene ontology (GO) enrichment analysis via RNA-seq demonstrated that the PLLCs biological processes, cellular components, and molecular functions were modified following $CoCl_2$ stimulation. (D) The top 10 GO-enriched terms were mostly associated with altered oxygen levels. (E) Kyoto encyclopedia of genes and genomes (KEGG) pathway analysis reveals PLLCs gene enrichment in the HIF-1 signaling pathway following $CoCl_2$ stimulation.

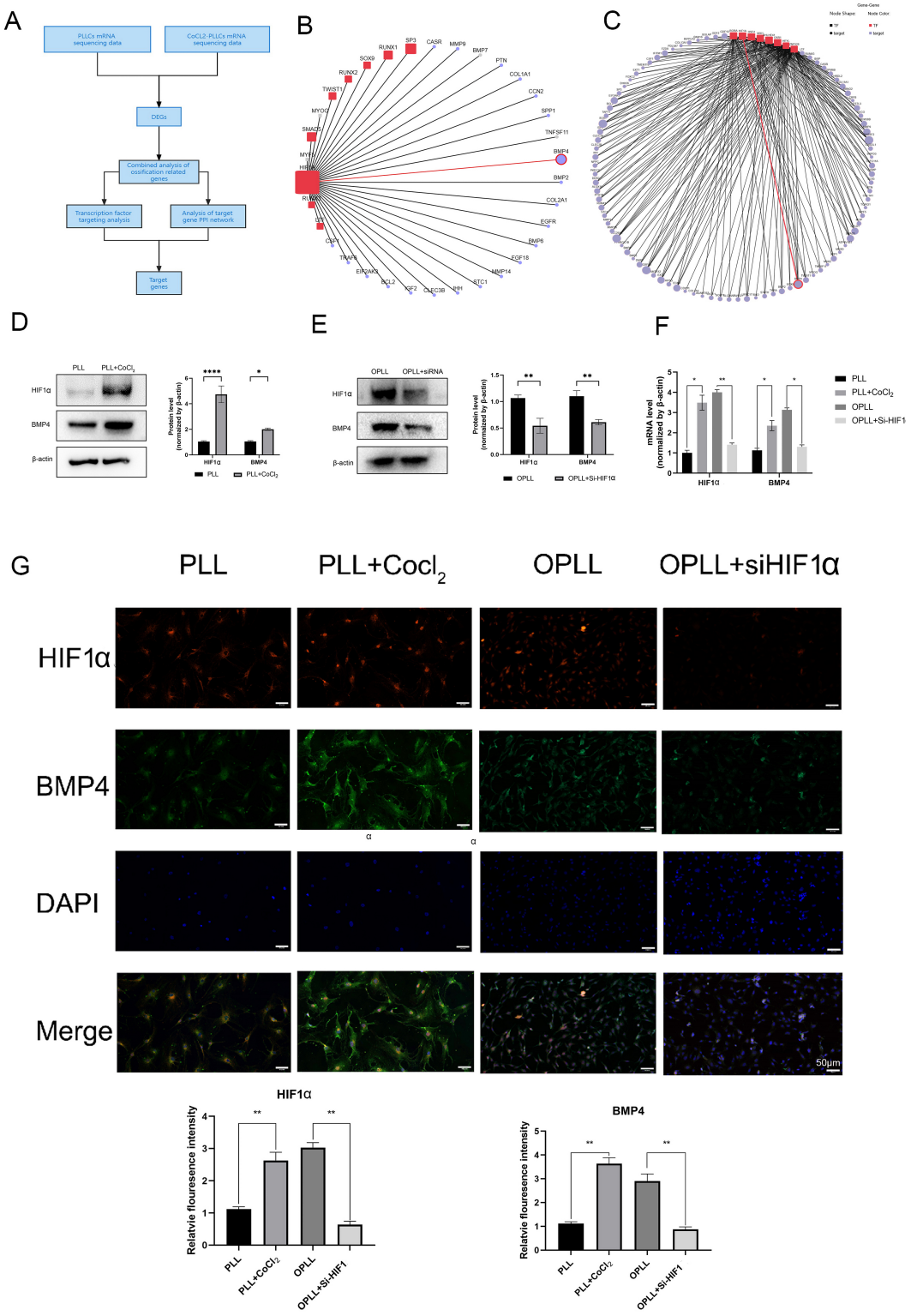

Fig. 5. HIF1A regulates BMP4 to promote ossification. (A) Flowchart of HIF1A target gene screening. (B) Differentially expressed ossification-associated proteins regulated by HIF1A. (C) Transcription factor targeting analysis. Squares represent transcription factors; circles represent transcription factor targets. (D) Representative western blots of HIF1A and BMP4 proteins from normal PLLCs and PLLCs treated with 100 μM $CoCl_2$ (n = 3/group). (E) Representative western blots of HIF1A and BMP4 proteins from normal OPLLCs and OPLLCs treated with short interfering RNA against HIF1A (n = 3/group). (F) Quantitative analysis of mRNA level expression (n = 3/group). (G) Cellular immunofluorescence staining results (n = 3/group). All experiments were performed in triplicate, and the data are the mean ± SEM; *$p < 0.05$, ** $p < 0.01$, **** $p < 0.0001$ within groups. Scale bar: 50 μm. BMP4, bone morphogenetic protein 4.

$CoCl_2$-stimulated PLLCs groups, specifically focusing on those categorized under the GO term "ossification" (GO: 0001503). Subsequently, we analyzed the target protein interaction network utilizing the STRING protein interactions database, with the results presented in Fig. 5A. Our findings indicated that HIF1A regulates the proteins of 32 ossification genes (Fig. 5B). Information regarding transcription factor binding motifs was obtained from the JASPAR database, and the target transcription genes were predicted using MEME FIMO (Fig. 5C). The relationship between transcription factors and target genes was illustrated through a transcription factor-target network diagram. Following this, we chose to further investigate BMP4.

The expression level of BMP4 protein increased in conjunction with the $CoCl_2$-induced upregulation of HIF1A (Fig. 5D). Western blot analysis revealed that BMP4 expression decreased following HIF1A knockdown ($p < 0.05$), correlating with reduced HIF1A levels (Fig. 5E). The mRNA expression and immunofluorescence results corroborated these earlier findings (Fig. 5F,G). Moreover, HIF1A was predominantly localized in the cytoplasm of PLLCs, while its expression in the nucleus increased after $CoCl_2$ stimulation, which was consistent with observations in OPLLCs.

4. Discussion

OPLL is a prevalent spinal disorder that has garnered significant attention due to its multifactorial etiology, which includes stress stimuli, genetic predispositions, and obesity. Despite the increasing recognition of OPLL as a serious health concern, the precise mechanisms that contribute to its development remain inadequately understood. This gap in knowledge highlights the urgent need for further investigation into the pathophysiological processes that underlie the expansion of ossified material within the spinal column. Currently, conservative treatment options for OPLL are limited, underscoring the necessity for mechanistic studies that can elucidate the biological processes involved in ossification and potentially prevent re-ossification after surgical interventions.

In our present study, we focused on the characterization of progenitor cells derived from patients with OPLL, specifically examining cells obtained from both normal and ossified PLLs. Our findings revealed that these progenitor cells exhibit specific MSC-like properties, characterized by the expression of surface antigenic markers typically associated with MSCs. Furthermore, these cells demonstrated the capacity for differentiation into osteoblastic and chondrogenic lineages, indicating their potential role in the ossification process. Notably, we observed that the ligament cells derived from OPLL patients exhibited enhanced osteogenic differentiation capabilities compared to their normal counterparts. This observation raises important questions regarding the underlying mechanisms that contribute to the increased osteogenic potential of ligament cells in individuals affected by OPLL, warranting further investigation to elucidate these processes.

Hypoxia, a condition characterized by reduced oxygen availability, has been shown to regulate various forms of HO, including both genotypic and acquired types. Our results confirm that hypoxia also plays a significant role in modulating the pathophysiology of OPLL. We observed differential expression of HIF1A in both PLL and OPLL tissues, as well as in primary cells derived from these tissues. This finding aligns with previous studies [27,28] that have reported similar patterns of HIF1A expression in other disorders associated with HO. To simulate hypoxic conditions in our experimental setup, we utilized $CoCl_2$, a well-established chemical hypoxia mimetic. We characterized the osteogenic potential of the cells through ARS and ALP staining, which are standard assays for assessing mineralization and osteogenic differentiation, respectively. The results demonstrated a significant increase in HIF1A expression in PLL cells following hypoxic treatment, which was accompanied by enhanced ossification, further supporting the role of hypoxia in the pathogenesis of OPLL.

To further investigate the functional role of HIF1A in OPLL, we employed siRNA to knock down HIF1A expression in OPLL cells. This intervention resulted in a corresponding decrease in ossification, providing compelling evidence for the involvement of HIF1A in the ossification process. However, it is important to note that the effects of HIF1A on OPLL cells were not validated *in vivo*, which presents a limitation to our findings. To gain deeper insights into the molecular mechanisms by which hypoxia regulates OPLL, we conducted RNA sequencing to analyze the downstream targets of HIF1A. Previous reports have indicated that BMP4 may play a significant role in the pathogenesis of OPLL, particularly among Asian patients [15–18] . Our analysis suggests that HIF1A may regulate BMP4 expression, thereby influencing the ossification process in OPLL. We conducted preliminary validation of this hypothesis, confirming that HIF1A regulates BMP4 within the $CoCl_2$-induced hypoxic microenvironment.

Interestingly, we observed that hypoxia promoted HIF1A upregulation in normal PLL cells, yet the expression of HIF1A varied between the original PLL and OPLL tissues, as well as between PLLCs and OPLLCs. This discrepancy suggests that the cellular response to hypoxia may differ based on the pathological state of the tissue. We hypothesized that prolonged stress stimulation, potentially due to mechanical stress or inflammatory injury, might lead to the establishment of a hypoxic microenvironment that partially activates HIF1A expression. Conversely, we propose that additional regulatory factors, possibly including inflammatory cytokines or other signaling molecules, may also contribute to the modulation of HIF1A expression in the context of OPLL.

In summary, our study highlights the complex interplay between hypoxia, HIF1A, and the pathogenesis of

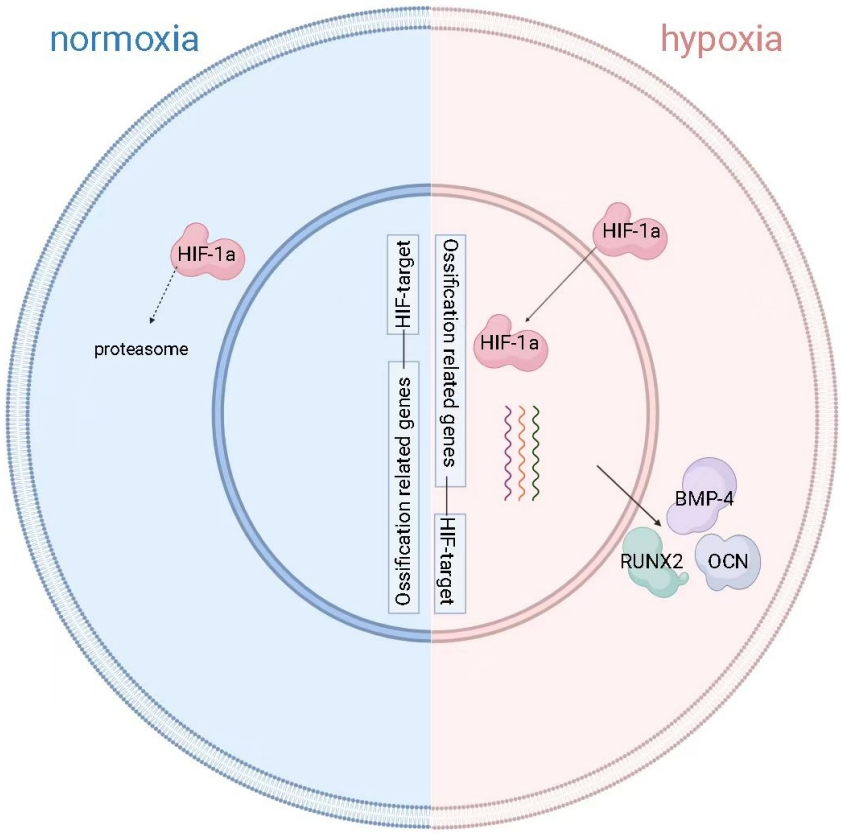

Fig. 6. Under normal conditions, HIF1A is degraded without entering the nucleus. Under hypoxic conditions, HIF1A enters the nucleus to regulate transcription and promote the expression of relevant ossification genes to promote OPLL. The image was drawn by the author via BioRender.com.

OPLL. The enhanced osteogenic differentiation capabilities of progenitor cells derived from OPLL patients, coupled with the differential expression of HIF1A, underscore the need for further research to elucidate the precise mechanisms driving ossification in this condition. Understanding these mechanisms may pave the way for the development of targeted therapeutic strategies aimed at preventing the progression of OPLL and improving patient outcomes. Future studies should focus on validating our findings *in vivo* and exploring the potential of HIF1A and BMP4 as therapeutic targets in the management of OPLL.

5. Conclusion

Primary cells derived from normal PLL and OPLL exhibited MSC-like properties and were capable of osteogenic-adipogenic and chondrogenic differentiation, and the OPLLCs were more osteogenic. We report the possible involvement of HIF1A in OPLL development and investigated OPLL regulation by the HIF1A-BMP4 axis (Fig. 6).

Availability of Data and Materials

Data in this study can be obtained by request and with permission from the corresponding author.

Author Contributions

JL and SL contributed equally to this work. SL, JL and AX performed the research and collected and analyzed the data. ZW and CX collected clinical samples and provided technical assistance. JY, JS and YL all performed manuscript writing checks and reviews, as well as participated in the design of the experiments, completing some of the experiments as well as data processing and reviews. All authors contributed to editorial changes in the manuscript. All authors read and approved the final manuscript. All authors have participated sufficiently in the work and agreed to be accountable for all aspects of the work.

Ethics Approval and Consent to Participate

The study was conducted according to the Declaration of Helsinki and approved by the Shanghai Changzheng Hospital Biomedical Research Ethics Committee (batch number: 2021SL044). All participants or their families/legal guardians gave written informed consent.

Acknowledgment

Not applicable.

Funding

This research was supported by grants from the National Natural Science Foundation of China (81972090).

Conflict of Interest

The authors declare no conflict of interest.

References

[1] Wu JC, Chen YC, Huang WC. Ossification of the Posterior Longitudinal Ligament in Cervical Spine: Prevalence, Management, and Prognosis. Neurospine. 2018; 15: 33–41. https://doi.org/10.14245/ns.1836084.042.

[2] Edwards DS, Clasper JC. Heterotopic ossification: a systematic review. Journal of the Royal Army Medical Corps. 2015; 161: 315–321. https://doi.org/10.1136/jramc-2014-000277.

[3] Shore EM, Kaplan FS. Inherited human diseases of heterotopic bone formation. Nature Reviews. Rheumatology. 2010; 6: 518–527. https://doi.org/10.1038/nrrheum.2010.122.

[4] Kim KS. Clinical Effectiveness of Posterior Cervical Decompression and Fusion in Terms of Reducing OPLL Growth Versus Cervical Motion Preservation. Neurospine. 2019; 16: 492–493. https://doi.org/10.14245/ns.19edi.012.

[5] Chen LF, Tu TH, Chen YC, Wu JC, Chang PY, Liu L, *et al*. Risk of spinal cord injury in patients with cervical spondylotic myelopathy and ossification of posterior longitudinal ligament: a national cohort study. Neurosurgical Focus. 2016; 40: E4. https://doi.org/10.3171/2016.3.FOCUS1663.

[6] Bernstein DN, Prong M, Kurucan E, Jain A, Menga EN, Riew KD, *et al*. National Trends and Complications in the Surgical Management of Ossification of the Posterior Longitudinal Ligament (OPLL). Spine. 2019; 44: 1550–1557. https://doi.org/10.1097/BRS.0000000000003127.

[7] Xu R, Hu J, Zhou X, Yang Y. Heterotopic ossification: Mechanistic insights and clinical challenges. Bone. 2018; 109: 134–142. https://doi.org/10.1016/j.bone.2017.08.025.

[8] Abiola R, Rubery P, Mesfin A. Ossification of the Posterior Longitudinal Ligament: Etiology, Diagnosis, and Outcomes of Nonoperative and Operative Management. Global Spine Journal. 2016; 6: 195–204. https://doi.org/10.1055/s-0035-1556580.

[9] Huang Y, Wang X, Lin H. The hypoxic microenvironment: a driving force for heterotopic ossification progression. Cell Communication and Signaling: CCS. 2020; 18: 20. https://doi.org/10.1186/s12964-020-0509-1.

[10] Wang H, Lindborg C, Lounev V, Kim JH, McCarrick-Walmsley R, Xu M, *et al*. Cellular Hypoxia Promotes Heterotopic Ossification by Amplifying BMP Signaling. Journal of Bone and Mineral Research: the Official Journal of the American Society for Bone and Mineral Research. 2016; 31: 1652–1665. https://doi.org/10.1002/jbmr.2848.

[11] Lin L, Shen Q, Leng H, Duan X, Fu X, Yu C. Synergistic inhibition of endochondral bone formation by silencing Hif1α and Runx2 in trauma-induced heterotopic ossification. Molecular Therapy: the Journal of the American Society of Gene Therapy. 2011; 19: 1426–1432. https://doi.org/10.1038/mt.2011.101.

[12] Kawao N, Yano M, Tamura Y, Okumoto K, Okada K, Kaji H. Role of osteoclasts in heterotopic ossification enhanced by fibrodysplasia ossificans progressiva-related activin-like kinase 2 mutation in mice. Journal of Bone and Mineral Metabolism. 2016; 34: 517–525. https://doi.org/10.1007/s00774-015-0701-3.

[13] Muñoz-Sánchez J, Chánez-Cárdenas ME. The use of cobalt chloride as a chemical hypoxia model. Journal of Applied Toxicology: JAT. 2019; 39: 556–570. https://doi.org/10.1002/jat.3749.

[14] Rovetta F, Stacchiotti A, Faggi F, Catalani S, Apostoli P, Fanzani A, *et al*. Cobalt triggers necrotic cell death and atrophy in skeletal C2C12 myotubes. Toxicology and Applied Pharmacology. 2013; 271: 196–205. https://doi.org/10.1016/j.taap.2013.05.005.

[15] Meng XL, Wang H, Yang H, Hai Y, Tian BP, Lin X. T allele at site 6007 of bone morphogenetic protein-4 gene increases genetic susceptibility to ossification of the posterior longitudinal ligament in male Chinese Han population. Chinese Medical Journal. 2010; 123: 2537–2542.

[16] Furushima K, Shimo-Onoda K, Maeda S, Nobukuni T, Ikari K, Koga H, *et al*. Large-scale screening for candidate genes of ossification of the posterior longitudinal ligament of the spine. Journal of Bone and Mineral Research: the Official Journal of the American Society for Bone and Mineral Research. 2002; 17: 128–137. https://doi.org/10.1359/jbmr.2002.17.1.128.

[17] Liu J, Chen Y, Shan X, Wang H. Investigation of the biomarkers involved in ectopic ossification: The shared mechanism in ossification of the spinal ligament. Frontiers in Genetics. 2022; 13: 991834. https://doi.org/10.3389/fgene.2022.991834.

[18] Ren Y, Feng J, Liu ZZ, Wan H, Li JH, Lin X. A new haplotype in BMP4 implicated in ossification of the posterior longitudinal ligament (OPLL) in a Chinese population. Journal of Orthopaedic Research: Official Publication of the Orthopaedic Research Society. 2012; 30: 748–756. https://doi.org/10.1002/jor.21586.

[19] Chang J, Yang B, Zhou Y, Yin C, Liu T, Qian H, *et al*. Acute Methylmercury Exposure and the Hypoxia-Inducible Factor-1α Signaling Pathway under Normoxic Conditions in the Rat Brain and Astrocytes *in Vitro*. Environmental Health Perspectives. 2019; 127: 127006. https://doi.org/10.1289/EHP5139.

[20] Zheng H, Wang N, Li L, Ge L, Jia H, Fan Z. miR-140-3p enhanced the osteo/odontogenic differentiation of DPSCs via inhibiting KMT5B under hypoxia condition. International Journal of Oral Science. 2021; 13: 41. https://doi.org/10.1038/s41368-021-00148-y.

[21] Wang Z, Gerstein M, Snyder M. RNA-Seq: a revolutionary tool for transcriptomics. Nature Reviews. Genetics. 2009; 10: 57–63. https://doi.org/10.1038/nrg2484.

[22] Hrdlickova R, Toloue M, Tian B. RNA-Seq methods for transcriptome analysis. Wiley Interdisciplinary Reviews. RNA. 2017; 8: 10.1002/wrna.1364. https://doi.org/10.1002/wrna.1364.

[23] Zhang H, He L, Cai L. Transcriptome Sequencing: RNA-Seq. Methods in Molecular Biology (Clifton, N.J.). 2018; 1754: 15–27. https://doi.org/10.1007/978-1-4939-7717-8_2.

[24] Withanage MHH, Liang H, Zeng E. RNA-Seq Experiment and Data Analysis. Methods in Molecular Biology (Clifton, N.J.). 2022; 2418: 405–424. https://doi.org/10.1007/978-1-0716-1920-9_22.

[25] Ayturk U. RNA-seq in Skeletal Biology. Current Osteoporosis Reports. 2019; 17: 178–185. https://doi.org/10.1007/s11914-019-00517-x.

[26] Athanasios A, Charalampos V, Vasileios T, Ashraf GM. Protein-Protein Interaction (PPI) Network: Recent Advances in Drug Discovery. Current Drug Metabolism. 2017; 18: 5–10. https://doi.org/10.2174/1389200218011701190204832.

[27] Li P, Zhang W, Zhang J, Liu J, Fu J, Wei Z, *et al*. Macrophage migration inhibitory factor promotes heterotopic ossification by mediating ROS/HIF-1α positive feedback loop and activating Wnt/β-catenin signaling pathway. Bone. 2025; 190: 117331. https://doi.org/10.1016/j.bone.2024.117331.

[28] Chen C, Song C, Liu B, Wang Y, Jia J, Pang K, *et al*. Activation of BMP4/SMAD pathway by HIF-1α in hypoxic environment promotes osteogenic differentiation of BMSCs and leads to ectopic bone formation. Tissue & Cell. 2024; 88: 102376. https://doi.org/10.1016/j.tice.2024.102376.